sustainability

MDPI

Article

Setting Key Model Parameters for Microscopic Traffic Simulation Using Vehicle Trajectory Data

Lorenzo Sica, Francesco Deflorio *, Matteo Ferraro and Giuseppe Calcagno

Department of Environment, Land and Infrastructure Engineering (DIATI), Politecnico di Torino, Corso Duca degli Abruzzi 24, 10129 Torino, Italy; lorenzo.sica@polito.it (L.S.); matteo.ferraro@polito.it (M.F.); giuseppe.calcagno@polito.it (G.C.)

* Correspondence: francesco.deflorio@polito.it

Abstract

Microscopic traffic simulation represents one of the most popular tools for analysing and comparing traffic performance in different scenarios of urban mobility. The reproduction of real-world traffic dynamics is its primary requirement for providing time-dependent estimates. This study presents a process to build a microscopic traffic model for an urban area of Athens, developed using high-resolution vehicle trajectories obtained from the pNEUMA dataset. Based on drone-recorded trajectories, a simulation scenario was built, combining a realistic road network model, including traffic light regulation, an estimated traffic demand, and a set of parameters to replicate the observed vehicle behaviour. The modelling process relies on an iterative comparison between simulated outputs and observed vehicle-level trajectory data. The proposed approach evaluates travel time distributions and helps develop an improved model, enhancing its ability to replicate the vehicle's behaviour. The final calibrated configuration reduced the Wasserstein distance by approximately 55.8% compared with the default SUMO configuration. The results also show that the calibration of microscopic behavioural parameters can substantially affect secondary simulation outputs, including emission estimates relevant for sustainability-oriented traffic analyses.

Keywords: traffic simulation; calibration; trajectories; microscopic simulation; emissions

1. Introduction

Accurate simulation scenarios enable researchers and practitioners to explore traffic dynamics in a controlled environment, test management policies, and introduce new technologies in a safe and replicable manner. They are also increasingly relevant for sustainability-oriented assessments, where simulated vehicle trajectories can be used to estimate environmental indicators such as emissions and fuel consumption under different traffic conditions. For these simulations to be truly useful and reliable, it is essential that the underlying scenarios reproduce real-world conditions with the highest possible degree of realism. In recent years, the growing availability of high-resolution vehicle trajectory data, e.g., coming from GNSS applications, has opened new opportunities for building data-driven simulation scenarios. These data not only support the modelling of road networks and traffic demand but also allow for a detailed comparison between simulated outputs and real-world observations using detailed or aggregated traffic statistics, such as distributions of travel times. This study presents the process of constructing a traffic simulation scenario in the urban area of Athens, based on real vehicle trajectory data and implemented using the SUMO (Simulation of Urban Mobility) microsimulation

Academic Editors: Natalia Distefano, Salvatore Leonardi and Maria Grazia Augeri

Received: 25 May 2026
Revised: 4 July 2026
Accepted: 8 July 2026
Published: 15 July 2026

environment. The first phase of the work requires the network definition, with some refinements of connections of the junctions, the demand generation from observed data, and a cleaning process of anomalous records. Although the obtained model is capable of reproducing route structures and spatial traffic distributions with an acceptable degree of realism, considering aggregated traffic indicators, some improvement in capturing temporal dynamics can be further implemented. Specifically, based on the observation, the present work introduces a targeted calibration procedure aimed at refining simulated vehicle behaviour to reduce the discrepancy between simulated and observed traffic flows. The main contribution of this study lies in the application of a structured, data-driven procedure for calibrating behavioural parameters in SUMO, with the goal of improving the travel time estimations of the simulated vehicles. The results demonstrate clear improvements over typical parameter configurations, proposing a new set of parameters for the calibrated model that can be used in similar simulation scenarios.

1.1. Related Works

This section reviews existing literature relevant to the construction and calibration of microscopic traffic simulation models, with a particular focus on the role of high-resolution trajectory data. The review is structured along three main lines: (i) technologies and methods for acquiring and applying vehicle trajectory data, (ii) modelling and calibration techniques within microscopic traffic simulators, and (iii) approaches for building urban-scale simulation environments, including digital twins. Together, these works provide the foundation for the modelling workflow proposed in this paper and highlight the key methodological gaps it aims to address.

1.1.1. Trajectory Data: Acquisition Technologies and Applications

The extraction of vehicular trajectory data is a key component in constructing advanced virtual models for traffic simulation. Several technologies have been developed for this purpose, each with specific advantages and limitations depending on the context and application needs. Among these, GPS is one of the most widely used, due to its ability to collect georeferenced data over large areas. Through GPS tools, vehicular trajectories can be reconstructed by processing geospatial and temporal point data [1–4]. This methodology is widely used for large-scale traffic analysis and allows the collection of large amounts of data in relatively short time. However, GPS has significant limitations in terms of accuracy, especially in congested urban settings [5,6]. In parallel, many extraction techniques are based on direct observation through instruments installed on road infrastructure, such as poles or bridges. Among these, radar sensors are widely used to detect objects and measure speed and distance. Radars offer significant advantages, especially in adverse weather conditions such as rain or fog, which may compromise other technologies. However, the limited resolution of data collected with radars reduces the ability to capture complex details in traffic behaviour [7,8]. To overcome these limitations, LiDAR (Light Detection and Ranging) technology offers an advanced solution based on the emission of laser pulses. LiDAR enables the generation of high-resolution three-dimensional data, which is ideal for monitoring vehicles and pedestrians in high-density urban areas [9,10]. Despite its potential, large-scale adoption of LiDAR is hampered by high costs and complex computational requirements. One alternative is the roadside acquisition of video images, followed by processing with computer vision algorithms that enable the identification and tracking of vehicles with high accuracy [11,12]. However, video detection technologies can be limited by narrow fields of view and the presence of blind sectors. To address these issues, solutions based on aerial sensing systems, such as Unmanned Aerial Systems (UAS), are emerging [13–17]. The pNEUMA dataset [18] used in this paper was, in fact, collected by drones equipped with high-quality video imaging instrumentation that performed collection campaigns flying over defined urban areas of the city of Athens. In addition to pNEUMA, other significant applications include the use of UAVs to monitor traffic flows both in urban environments [19] and on highways or extra-urban contexts, where the panoramic view allows tracking vehicles on multiple lanes simultaneously [20–22]. Vehicular trajectory data have applications in multiple areas, with a central role in understanding and optimising traffic dynamics. Among these, a particularly significant use is in the analysis of users' driving behaviour [23,24]. Through detailed trajectory observations, it is possible to study phenomena such as car-following [25,26] and lane-changing [27–29], which are key elements in modelling vehicle interactions under varying traffic conditions and accurately replicate individual and collective behaviours on the road. Trajectory data also play a key role in identifying abnormal behaviour, such as abrupt braking, sudden acceleration, or irregular speed changes [30,31]. This information is crucial for enhancing road safety and pinpointing trouble spots in road networks. Another relevant application is in traffic flow monitoring, which utilises trajectory data to analyse and predict congestion, thereby improving urban mobility management and supporting navigation and route optimisation systems [32–34]. While trajectory data are valuable in their own right, their full potential emerges when they serve as input for the construction and calibration of models in traffic simulation environments. However, in many existing studies, trajectory data are still primarily used for aggregate validation, rather than for the systematic calibration of microscopic behavioural parameters at the individual-vehicle level.

1.1.2. Modelling and Calibration in Microscopic Simulation

Microscopic traffic simulations rely on behavioural assumptions to replicate real-world dynamics with acceptable fidelity. To bridge the gap between default simulator settings and observed traffic behaviour, recent research has increasingly focused on systematic calibration of behavioural parameters. These typically encompass parameters related to longitudinal control, lane-changing decisions, vehicle dynamics, and stochastic elements of driver attitude. Calibration practices vary considerably, reflecting not only methodological choices but also the constraints and capabilities of the particular microscopic simulation environment used. Several studies have addressed calibration through direct comparison of simulation outputs with field observations. Ref. [35] performed calibration of car-following parameters defined in SUMO by minimising the RMSE of travel time and queue lengths in a congested urban setting. Similarly, Ref. [36] used TransModeler to replicate vehicle merging on highway acceleration lanes, demonstrating that behavioural modelling can reveal significant mismatches with geometric design standards. In both cases, calibration was crucial to enhance the alignment between simulated and observed traffic operations. Other studies have employed sensitivity analysis and statistical modelling. Ref. [37] analysed the impact of parameter uncertainty on simulation accuracy using AIMSUN, finding that reaction time and minimum distance significantly affect travel time outputs. Sensitivity analysis has also been used by [38] in other simulation-based transport applications to identify influential input variables and support the exploration of computationally demanding parameter spaces. A complementary approach is proposed by Punzo and Montanino (2016) [39], who argue that calibrating models on cumulative spatial variables (e.g., position) yields better residual dynamics than calibration based on instantaneous speed, especially for car-following models like the IDM. From a safety-oriented perspective, Ref. [40] showed that microscopic traffic models calibrated using standard performance indicators may still exhibit significant local inconsistencies at the conflict level, highlighting the need for complementary microscopic validation beyond aggregate measures. Optimisation-based methods represent another step forward. Ref. [41] applied genetic algorithms to calibrate

VISSIM parameters under heterogeneous traffic conditions [42]. Further expanded this line by combining global and local parameter tuning using ANOVA and recursive grouping techniques. Their results, based on the NGSIM dataset, show how point-distribution calibration outperforms single-value matching, particularly when using metrics like MAPE and Kullback–Leibler divergence. Similarly, Ref. [43] proposed a genetic algorithm-based calibration framework with vehicle class-specific parameters, showing that differentiating behavioural parameters across vehicle categories can significantly improve travel time replication in heterogeneous traffic conditions. Recent urban applications also confirm the practical relevance of calibrated simulation models for evaluating traffic management strategies. For instance, Ref. [44] developed a calibrated mesoscopic model for a congested commercial district using field traffic data and validated the model through statistical indicators before assessing alternative traffic interventions. Such studies underline the importance of calibration and validation in applied traffic simulation, while also showing that many evaluation procedures remain centred on aggregate performance indicators. The integration of high-resolution trajectory data has played a key role in these advancements. Ref. [45] utilised detailed vehicle paths to calibrate lane-changing and gap-acceptance models, revealing that traditional planning rules on access spacing may not be applicable under consistent traffic demand. Ref. [46] incorporated 3D LiDAR-derived trajectories to calibrate both car-following and lane-changing behaviours in VISSIM, demonstrating that such calibration improves safety assessment through surrogate measures. In addition to accuracy, computational efficiency is becoming a growing concern. Ref. [47] addressed this by proposing a co-simulation framework that combines microscopic details near ego vehicles with mesoscopic wave-propagation models for distant traffic, achieving performance gains without significantly sacrificing behavioural realism. Lastly, calibration has also been extended to support safety-focused applications. Ref. [48] introduced a novel method using Extreme Value Theory (EVT) to align simulated and observed distributions of traffic conflicts. This approach outperformed correlation-based calibration when predicting crash-related indicators, highlighting the importance of aligning statistical tail behaviour for risk estimation. Calibrated behavioural models become the foundation for constructing realistic digital environments, enabling the simulation of complex traffic dynamics and the testing of intervention strategies under diverse conditions. However, many existing approaches still rely on aggregate performance metrics, limiting their ability to reproduce individual-level patterns.

1.1.3. Building Urban Traffic Models

In this context, advanced virtual environments for traffic scenarios can be essential tools to support the applications described, providing dynamic simulations that integrate real-time information to model traffic flows, driving behaviours, and future scenarios. Using these tools, it is possible to replicate actual traffic conditions and virtually test innovative mobility strategies, such as the introduction of autonomous vehicles. Additionally, they enable in-depth analyses of driver willingness to enhance road safety and infrastructure planning. Several experiences in building traffic microsimulation models are documented in the literature, highlighting different methodological approaches and specific applications. In Ref. [49], the construction of an urban traffic scenario in the case study of Barcelona is proposed. As in this paper, the simulation was implemented using the SUMO software, and the road network was constructed from OpenStreetMap data. In this case, traffic demand was assigned through origin-destination matrices derived from mobile phone data and integrated with mobility surveys. This represents a major difference from the methodology proposed in this paper, which is based on the direct route assignment of individual observed trips. Several similar experiments propose constructing microsimulation models for fairly large areas, such as entire urban areas [50–52]. In Ref. [53], a microsimulation model is proposed for the study area of Bologna (Italy) by assigning traffic to the SUMO tool through an integration of flows derived from GPS data and O/D matrices to calibrate vehicle flows on the road network extracted from OpenStreetMap. Other studies [54–56] instead propose models limited to narrower areas, as in the case of our paper, where a microsimulation model succeeds most effectively. For instance, an automated method for traffic modelling is presented in Wang et al. (2022) [57], aimed at creating digital twins in localised traffic scenarios that are ideal for analysing autonomous vehicle capabilities. There are also Other studies in the literature that propose the construction of twin models on suburban highway sections [57–59]. Previously reported experiments focus on experiments in which traffic demand generation is derived from static data, assigned directly or through models calibrated to these observations. However, a significant development is the continuous updating of digital twin models through real-time processing of dynamically collected data. Various examples of edge-to-cloud applications are available in the literature, where real-time data is processed by learning algorithms to build and continuously update digital traffic models [60,61]. In Ref. [62], a traffic model powered by road sensor and camera data was showcased, integrated with deep learning algorithms optimised for traffic sign recognition and real-time traffic monitoring via edge computing.

1.2. Discussion and Positioning of the Present Work

The explored literature reveals that recent advancements in data collection technologies, modelling techniques, and simulation environments have greatly expanded the possibilities for data-driven traffic analysis. While previous research has made significant progress in data collection, simulation modelling, and calibration techniques, important gaps remain. In particular, high-resolution trajectory data are still underutilised for building calibrated traffic simulations in dense and heterogeneous urban environments. Moreover, validation procedures tend to rely on aggregate metrics, often neglecting the internal variability of travel patterns. This study contributes to addressing these gaps by implementing a distribution-based calibration approach using drone-collected urban trajectory data. By comparing the full distributions of simulated and observed travel times, rather than just average values, the method enables a more precise calibration of behavioural parameters. This study therefore focuses on the development and assessment of a data-driven pipeline that transforms high-resolution vehicle trajectories into a calibrated microscopic simulation scenario. The central objective is to show how trajectory data can support the construction of the road network, demand, signal settings, and behavioural parameter configuration in a coherent modelling workflow. Within this pipeline, distribution-based calibration and class-specific parameter tuning are used as methodological components to improve the reproduction of observed traffic dynamics compared with default simulator settings. The resulting scenario is then evaluated through disaggregated microscopic indicators and an independent temporal validation. Furthermore, the entire modelling pipeline is built on open tools and data, offering a replicable and scalable solution for detailed urban traffic analysis.

2. Methodology

The methodology adopted in this study is articulated in two main phases. In the first one, a base simulation scenario is defined using high-resolution trajectory data. This preliminary process includes the generation and refinement of the digital road network model, the estimation and direct derivation of traffic demand from observed vehicle trips, and the adjustment of traffic signal plans to reflect the real-world operational conditions. The second phase focuses on calibrating key vehicle behavioural parameters used in the microscopic traffic simulation environment to improve the model accuracy in travel time estimation for different vehicle types. The calibration process follows a stepwise, data-driven approach, evaluating the alignment between simulated and observed travel time distributions using the Wasserstein distance as the primary metric.

2.1. Traffic Scenario Construction

The construction of a microscopic traffic simulation scenario from empirical trajectory data requires a methodology to ensure consistency between observed and simulated dynamics. This process involves defining the road network and extracting vehicle demand from raw trajectory information. The road infrastructure is typically derived from open geographic datasets such as OpenStreetMap and subsequently refined to address geometric and topological inaccuracies that may arise from automatic procedures. Particular attention must be paid to the correctness of intersection layouts, lane connectivity, turn permissions, and priority rules. In urban streets, intersections often require manual adjustment to reflect real-world configurations and avoid simulation artefacts such as unrealistic queuing or vehicle teleportation. As part of this network refinement phase, traffic signal plans must also be specified. When direct information on signal timings is unavailable, fixed-cycle control schemes can be inferred by analysing vehicle stopping patterns observed in the trajectory data. Traffic demand is instead derived directly from the observed trajectories. This step involves mapping each trajectory to a sequence of network edges, preserving the original departure time, vehicle type, and route. The use of trajectory-based demand avoids the need for aggregated origin-destination models and retains the empirical structure of traffic flow. Accurate spatial matching between GPS points and network elements is crucial for maintaining route fidelity, particularly in complex urban areas. When properly implemented, this methodology yields a base simulation scenario that reproduces the spatial structure of traffic operations with an acceptable level of realism, serving as a preliminary platform for behavioural calibration and further analysis.

2.2. Calibration Approach

Once the base scenario has been constructed, the further methodological phase involves calibrating behavioural parameters to enhance the alignment between simulated and observed traffic dynamics. In this study, calibration focuses specifically on the time dimension of traffic performance, aiming to reduce the discrepancy between the distribution of simulated travel times for individual vehicles and those recorded in empirical trajectory data. A stepwise calibration strategy is adopted to manage model complexity and reduce computational burden. Parameters are grouped according to their functional role in the simulation: car-following model, vehicle dynamics, and speed preferences. Each group is calibrated sequentially, holding previously optimised parameters fixed during subsequent steps. This modular approach enhances interpretability and facilitates the isolation of the individual contribution of each parameter set to the overall model performance. The calibration process involves running batches of simulations in which selected parameters are varied across predefined ranges. For each configuration, simulation outputs are compared with observed data using a distribution-based metric. Rather than relying on aggregate indicators such as average travel time for traffic flow, the comparison is performed using the Wasserstein distance, which evaluates the full shape and spread of the travel time distributions for individual vehicles. This enables a more detailed and behaviorally consistent adjustment of the microscopic traffic model.

2.2.1. Parameter Selection and Sampling Strategy

The calibration process is structured around three groups of parameters, representing a specific aspect of how a vehicle reacts within the simulation environment. These groups are calibrated sequentially, allowing each step to progressively refine the model based on the corresponding behavioural component:

- Step 1—Car-Following, reaction and speed related parameters.
  This step focuses on parameters that define longitudinal vehicle interactions. Specifically, the calibration focuses on "tau" (reaction time) and "mingap" (minimum following distance), which are core elements of the Krauss car-following model. In parallel, "actionStepLength" is also calibrated; it directly affects how frequently vehicle behaviour is updated during simulation and therefore influences overall traffic dynamics. In addition, this step also includes the exploration of the parameter "speed factor", which modifies each vehicle's desired speed relative to the speed limit of the road segment, allowing the model to capture variability in driver aggressiveness or caution.
- Step 2—Variability parameters.
  The second calibration step focuses on the calibration of parameters related to variability in agents' behaviour. In particular, "sigma" defines driver imperfection generating differences in agents' driving ability. Also, "speedDev" is introduced. This parameter allows modelling the already defined "speedFactor" as a normal distribution characterised by its mean and standard deviation ("speedDev").
- Step 3—Vehicle's dynamic parameters.
  This final step addresses the physical performance limits of vehicles, calibrating "accel" (maximum acceleration) and "decel" (maximum deceleration), which play a key role in determining responsiveness and flow propagation under various traffic conditions.

In each step, the parameters under consideration are varied across predefined ranges derived from both the microsimulation tool's default values and scientific literature in the field. The ranges are selected to balance realism, plausibility, and computational feasibility. A full grid search strategy is employed, where all possible combinations of the selected parameter values are simulated to comprehensively explore the parameter space. Initially, in Step 1, the same parameter values are applied uniformly to all vehicle types. This unified phase enables coarse filtering of parameter effects, helping to identify values that are clearly suboptimal or optimal across the entire vehicle population. Subsequently, the calibration is refined by introducing class-specific parameter tuning. Vehicles are grouped into three categories: light vehicles (cars, taxis, and medium vehicles), motorcycles, and heavy vehicles (trucks and buses). Each class is then assigned its own set of parameters to better capture behavioural heterogeneity across vehicle types and contributes to improving the overall alignment between simulated and observed travel time distributions. In defining the calibration set, lane-changing parameters were excluded from the grid search. This choice was made to avoid an excessive increase in the dimensionality of the parameter space. Nevertheless, lateral behaviour was considered by using the default SUMO lane-changing model, with its standard parameters fixed throughout the calibration process. In particular, the model components related to strategic lane selection and cooperative interactions were retained to reproduce lane-use and interaction patterns, while their explicit calibration is left for future extensions of the proposed workflow.

2.2.2. Evaluation Metric: Wasserstein Distance

To assess the effectiveness of each simulation configuration, the distribution of travel times for all the simulated vehicles is compared with the distribution of times observed from the original trajectory data. Indeed, the proposed methodology does not rely on simpler aggregate comparison indicators such as average or median travel time, but adopts a distribution-based approach derived from vehicle-level trajectory data. This choice allows the calibration to exploit the disaggregated information provided by individual trajectories while focusing on the reproduction of the overall travel time distribution. The objective is therefore not to perform a direct vehicle-to-vehicle matching, but to calibrate a scenario that reflects the observed distributional properties of traffic dynamics. In particular, the Wasserstein distance was selected as the main comparison parameter. This metric quantifies the minimum effort required to transform one probability distribution into another, making it particularly suitable for comparing distributions that may differ in shape and dispersion, even when their central trends are similar.

Considering the two one-dimensional distributions s and r, the Wasserstein distance $W(s,r)$ is defined as

$$W(s,r) = \int_{-\infty}^{\infty} |S(x) - R(x)| dx$$

where $S(x)$ and $R(x)$ are the cumulative distribution functions of s and r respectively.

The use of the Wasserstein distance is motivated by its solid theoretical foundation and its recent application in statistical learning and empirical data comparison. Indeed, Wasserstein-based metrics provide a robust and interpretable framework for measuring distributional divergence in complex systems, including transport-related applications [63]. This metric was chosen over alternatives such as the Kolmogorov–Smirnov (KS) test because it is more sensitive to global differences in distribution shape and less affected by local deviations, especially in the tails. In preliminary experiments, the KS test showed limitations in capturing meaningful differences between distributions that had minor shifts in extreme values but were otherwise well aligned. The Wasserstein distance was computed using the "wasserstein_distance" function from the scipy.stats 1.18 library, applied to matched sets of observed and simulated travel times across all simulation configurations. By using this metric, we ensure a fast and interpretable evaluation of simulation accuracy, grounded in the full distributional structure of travel time data.

2.2.3. Implementation and Execution of Simulation Experiments

The calibration process was implemented through a systematic full-factorial grid search strategy, where all possible combinations of parameter values within predefined ranges were simulated and evaluated. This exhaustive approach enabled a comprehensive exploration of the full parameter space. Each calibration step was executed in isolation, following a cascaded structure: parameter groups were calibrated sequentially, while previously optimised values were held fixed in subsequent steps. This modular structure allowed for clear attribution of model behaviour to specific parameters. Simulations were carried out using the open-source microscopic traffic simulator SUMO, and the execution framework was developed in Python 3.14 to manage the simulation experiments. The code was designed to automate the generation of configuration files, launch simulation runs in sequence, and collect performance metrics. In each step, up to 10,000 simulations were executed to ensure a sufficiently granular evaluation of the parameter range. After each run, the resulting travel time distributions were extracted and compared to the empirical reference using the Wasserstein distance. The framework identified the parameter configuration that minimised the distance to the observed distribution, and the best-performing settings were carried forward to the next calibration step. In the final phase, this process was repeated independently for each vehicle class, enabling a targeted calibration that captured heterogeneity across vehicle types. The calibration simulations were performed on a VMware virtual machine equipped with an Intel Xeon w5-3435X processor, equipped in a workstation (Dell Inc., Round Rock, TX, USA), with 16 vCPUs, and 32 GB of RAM. To maximise computational efficiency, SUMO was run in single-thread mode, while process-level parallelism was achieved by executing up to 12 simulations concurrently. Processing 10,000 simulation runs for a calibration scenario required approximately 4–8 h, with an average execution time of 5–12 s per run. This includes an estimated hypervisor overhead of about 10% compared with bare-metal execution.

3. Dataset and Simulation Scenario Definition

The simulation scenario developed in this study is based on high-resolution vehicular trajectory data provided by the pNEUMA dataset [18]. This dataset was collected in the urban area of Athens through a large-scale field experiment conducted using Unmanned Aerial Vehicles (UAVs). The drones performed continuous aerial video recordings over multiple zones of the city, capturing vehicular movements with a temporal resolution of 25 Hz. The resulting trajectories contain detailed information for each vehicle, including timestamped positions, speeds, accelerations, and vehicle types. The high spatiotemporal resolution and coverage of the dataset make it particularly suitable for constructing microsimulation scenarios, especially for studying detailed driving patterns, vehicle interactions, and dynamic traffic conditions. For this study, a 15 min observation window was selected during the morning peak hour (from 08:30 to 09:00), focusing on one of the central zones (Zone 3) covered by pNEUMA (Figure 1).

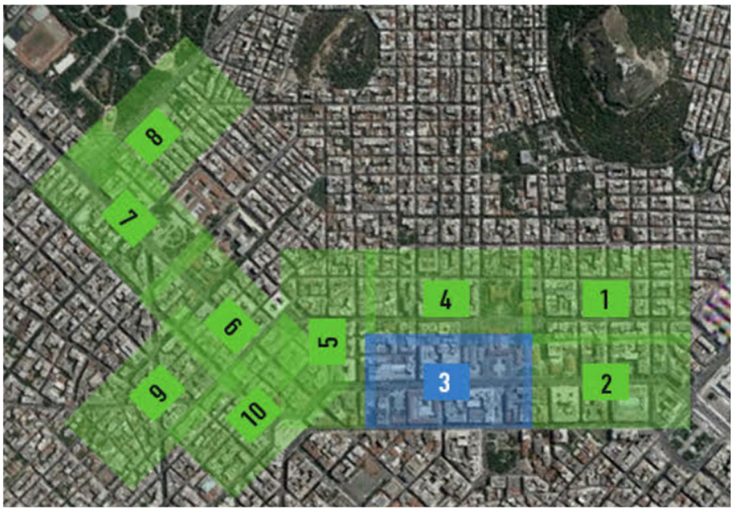

Figure 1. Extraction of zone 3 observations from pNEUMA dataset.

This subset includes 2112 vehicle trajectories, offering a dense yet manageable sample of urban traffic. Unlike traditional data sources such as origin-destination matrices or static traffic counts, trajectory data provides direct insight into individual trip patterns, including specific routes followed in time. Moreover, the dataset includes a vehicle-type-based classification (cars, buses, motorcycles, medium vehicles, heavy vehicles, taxis), enabling a differentiated modelling of vehicle dynamics. This level of detail enables a more realistic and behaviorally grounded simulation environment, where each trip can be faithfully reconstructed within the simulation.

The following paragraphs describe the operations that enabled the construction of a road network and traffic demand suitable for replicating the scenario observed in a microsimulation environment.

3.1. Road Network Construction and Refinement

The digital road network used for the simulation was initially generated using the OpenStreetMap (OSM) data via the SUMO Web Wizard tool. This automated procedure enables the extraction of road geometry corresponding to the selected study area, providing a basic yet structured representation of road segments, intersections, and priorities. However, while OSM data offers valuable coverage and open accessibility, the direct import into the microsimulation environment revealed several limitations in terms of road network fidelity and operational accuracy. The preliminary version of the network suffered from geometric inconsistencies, especially at intersections. In particular, several junctions presented incorrect layouts, misaligned connections, or unrealistic turning configurations that created severe traffic bottlenecks and simulation failures. One of the most critical issues was observed at a major signalised intersection along the primary arterial, where default imported geometry led to excessive congestion and unfeasible vehicle trajectories. Therefore, several adjustments have been implemented, including:

- Realignment and correction of intersection geometries (Figure 2);
- Verification and adjustment of lane connectivity and priorities;
- Restoration of turn permissions and prohibition rules.

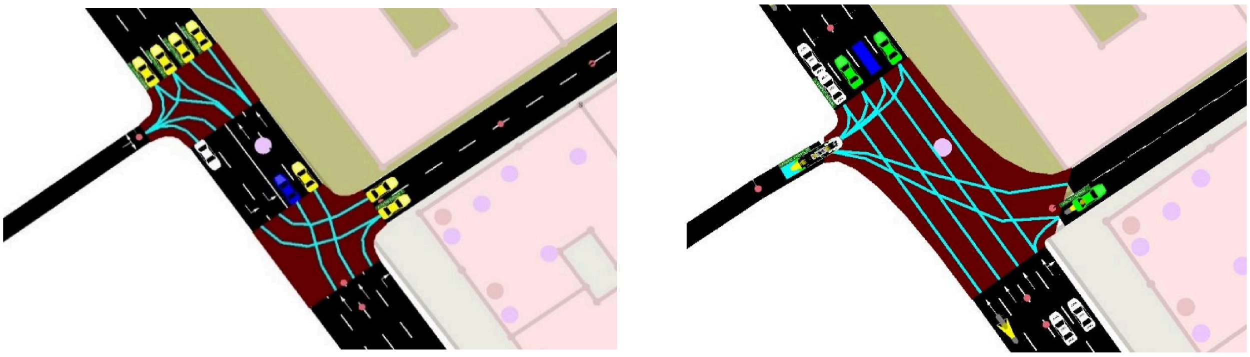

(**a**) (**b**)

Figure 2. Example of a critical Intersection imported (**a**) and edited (**b**).

Furthermore, it was essential to ensure that the network accurately reflected the conditions at the time of the data acquisition. Some parts of the real network had undergone changes in later years, such as the reduction in the number of lanes or the introduction of bus-only lanes, which were reversed to match the historical configuration corresponding to the pNEUMA dataset, which was collected in 2018. Following the corrections, a validation phase was performed through simulation test runs. These highlighted substantial improvements in vehicle flow consistency, reduction in teleportation events, and better alignment between the simulated and observed spatial dynamics. In the initial network setup, the traffic signal plans were automatically generated by SUMO based on imported OpenStreetMap data. These default signal configurations (typically fixed-cycle plans with symmetrical green phases) were often inconsistent with real-world traffic control strategies. As a result, several intersections exhibited unrealistic congestion patterns, particularly along the main arterials (Figure 3), where coordinated signal timing plays a crucial role in maintaining flow continuity.

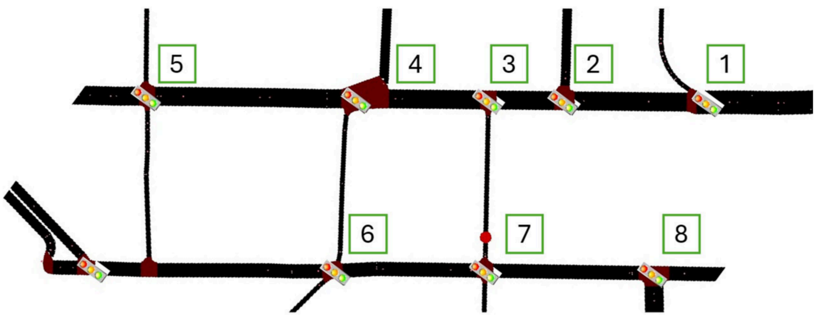

Figure 3. Positions of the 8 signalised intersections in the study area road network.

To address this, traffic signal programs were identified using a data-driven method. Time-space diagrams were constructed for vehicles approaching signalised intersections to detect stopping patterns and queue formation, and to estimate signal phases and durations. An example of traffic light timing identification using time-space diagrams is reported in Figure 4.

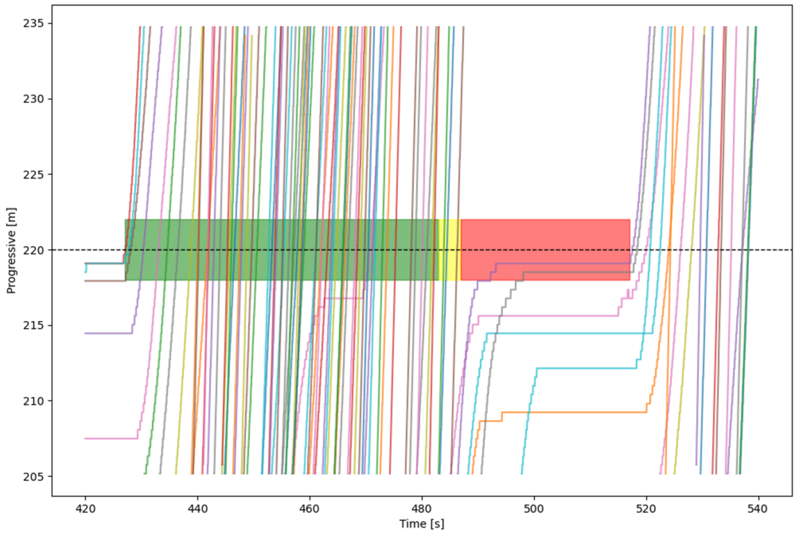

Figure 4. Example of traffic light cycle identification using vehicle trajectories in time-space diagrams, with green, yellow, and red durations.

The identification of signal timings was performed through a stepwise analysis of the observed trajectories. First, the signalised intersections located along the two main arterials were identified, and only the trajectories crossing the full arterial section were selected in order to observe repeated stopping and discharge patterns at consecutive intersections. Vehicle coordinates were then transformed into progressive distances along the reference road, and time–space diagrams were generated by plotting vehicle position against time. In these diagrams, signalised intersections were represented as fixed distance lines, while near-horizontal trajectory segments upstream of an intersection were interpreted as stopping and queue formation during red phases. The beginning of the green phase was inferred from the discharge of queued vehicles and their crossing of the stop line, whereas the beginning of the red phase was inferred from the onset of systematic stopping upstream of the intersection. Repeated patterns across different cycles and intersections were then used to estimate cycle length and green, yellow, and red durations. Finally, offsets were calculated by selecting a reference intersection with zero offset and estimating the time required to travel between consecutive intersections at the observed average progression speed, in order to reproduce the green-wave pattern visible in the trajectory diagrams. Following this procedure, a fixed cycle of 90 s was adopted for the signalised intersections along the main arterial roads, consisting of 56 s of green, 4 s of yellow, and 30 s of red for the main-road approaches. The estimated offsets between traffic control plans were then implemented in SUMO to reproduce a progression pattern consistent with the observations.

3.2. Traffic Demand Generation from Trajectories

The vehicle demand used in the simulation was derived directly from the individual trajectories included in the pNEUMA dataset. Each trajectory provides a complete record of a vehicle's motion across the study area, including its origin and destination, intermediate positions, timestamps, and vehicle type. This detailed structure enables a trip-by-trip reconstruction of vehicular demand. A matching algorithm was designed and implemented to associate each point in a trajectory to the nearest edge in the road network, while preserving the route geometry and temporal consistency. This required careful handling of spatial inaccuracies and mapping ambiguities, especially in zones with dense network elements or complex intersection layouts. The algorithm assigns each vehicle's entry and exit edge, departure time, and complete route as a sequence of lane segments. Each observed trajectory was converted into a SUMO-compatible trip definition by assigning the vehicle's departure time, entry and exit edges, and departure speed. A detailed analysis of the simulation and comparison with real data revealed that some vehicles, particularly motorcycles, were travelling stretches of road in the opposite direction of travel, which could not be replicated in the simulation due to the traffic rules implemented in the one-way edges of the model. An extreme example showed a vehicle with a real travel distance of 90 m but a simulated distance greater than 900 m, due to the circulation rules for travelling from one point to another available in the simulation (Figure 5).

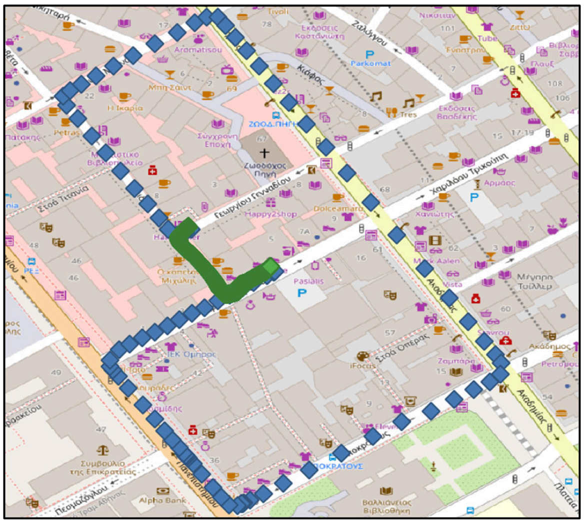

Figure 5. Observed (green) and simulated (blue) paths for a vehicle not following the traffic rules.

To avoid such errors, it was decided to exclude vehicles that did not comply with the road traffic rules (approximately 15, mostly motorcycles) from the simulation. This choice further reduced the discrepancies between simulated and observed data, improving the overall reliability of the model. The resulting configuration allowed for high-fidelity reproduction of the observed trajectories. Across the dataset, the average deviation in simulated travel distance remained below 5%, ensuring strong alignment between the simulation and the empirical data.

4. Results of Vehicle Behaviour Calibration and Discussion

The simulation scenario defined and described in Section 3 served as the baseline for the subsequent calibration of vehicle behavioural parameters. In this section, the results of the calibration process steps are presented and discussed, highlighting the impact of parameter values on the accuracy of the simulation.

4.1. Step 1—Calibration of Car-Following and Behavioural Parameters

The first step of the calibration process focused on investigating vehicle behavioural parameters related to longitudinal interactions, simulation update frequency and speed-related patterns. Given the specific nature of these parameters and the heterogeneity in driving manners across vehicle types, a two-phase approach was adopted: a general exploratory pre-calibration, followed by a more detailed and class-specific calibration.

4.1.1. Pre-Calibration: Exploratory Analysis and Range Refinement

The pre-calibration phase aimed to refine the initial parameter ranges before performing the main calibration. This process was divided into two sub-stages to progressively isolate the most influential factors.

In the first exploratory stage, only the parameter speedFactor was varied, while keeping all other parameters at their default SUMO values. This decision was motivated by the analysis of empirical traffic data collected in central Athens, which revealed that a substantial proportion of vehicles exceeded the posted 50 km/h speed limit. Consequently, speedFactor was considered a critical variable to reproduce the observed speed distribution. The exploration focused on identifying a scaling factor capable of reflecting the prevalent speeding behaviour without compromising the stability of the simulation. The value of the speedFactor defined after an iterative procedure was 1.6. The interpretation of this value requires considering the role of this parameter within the SUMO vehicle model. Rather than representing the speed actually reached by each vehicle, speedFactor defines the desired-speed multiplier applied under free-flow conditions, while actual speeds remain constrained by car-following interactions, acceleration and deceleration limits, traffic signals, queues, and local network conditions. To support the selected value, Figure 6 reports the empirical distribution of observed instantaneous speeds in the calibration scenario. The distribution shows that, although most observations remain below the nominal 50 km/h limit, a visible tail exceeds this threshold, indicating the presence of higher-speed observations during less constrained conditions.

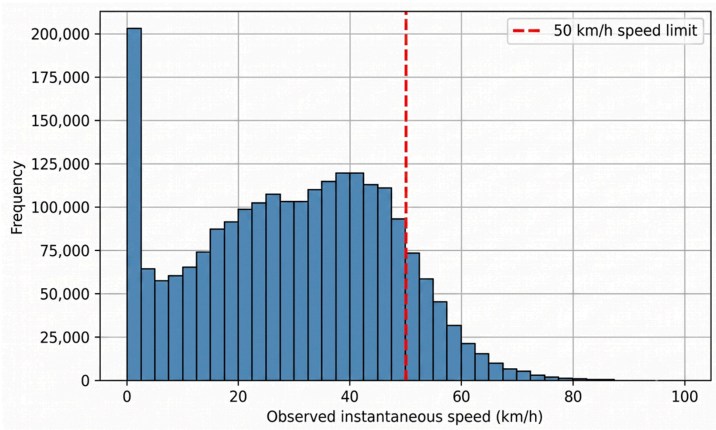

Figure 6. Observed instantaneous speed distribution.

In the second exploratory stage, once the speedFactor had been identified, the calibration process incorporated variations in the remaining three parameters: minGap (minimum following distance), tau (driver reaction time), and actionStepLength (update frequency of vehicle dynamics). This stage allowed for identifying minGap = 3 m as the most consistent value across different configurations and traffic densities, showing robust convergence compared to alternative settings. The results also served to narrow and centre the feasible search intervals for tau and actionStepLength, improving the efficiency of the subsequent main calibration phase.

4.1.2. Main Calibration: Class-Specific Parameter Tuning

Building on the insights from the pre-calibration phase, the main calibration campaign focused exclusively on the parameters tau and actionStepLength. Unlike the initial exploration, this stage adopted a class-specific approach, testing separate configurations for light vehicles (cars, taxis, and medium-sized vehicles), motorcycles, and heavy vehicles (trucks and buses). This distinction was introduced to capture the behavioural heterogeneity observed across vehicle categories, while keeping the computational demand at a reasonable level. A constraint was introduced whereby actionStepLength could not exceed tau, ensuring consistency between the temporal resolution of driver reactions and the update frequency of the simulation engine. When actionStepLength is greater than tau, vehicles react with a delay relative to the defined safety distance, which leads to unrealistic acceleration spikes and collisions. The constraint guarantees at least one behavioural update within each headway interval, improving both model stability and realism of simulated traffic dynamics. Table 1 summarises the explored parameter ranges in the pre-calibration and main calibration phases. The preliminary step helped refine the search intervals, notably shifting the range of actionStepLength toward higher precision values.

Table 1. Tested range of parameter values selection.

Parameter	Description	Default SUMO	Tested Range (Pre-Step)	Tested Range (Step 1)
tau	Reaction time	1.0 s	0.5–1.2 (step 0.1)	0.6–0.9 (step 0.1)
actionStepLength	Vehicle update frequency	1.0 s	0.5–1.1 (step 0.1)	0.5–0.8 (step 0.1)
speedFactor	Vehicle's desired speed	1.0	0.8–2.0 (step 0.2)	Fixed at 1.6
minGap	Minimum following distance	2.5 m	1.5–3.5 (step 0.5)	Fixed at 3.0

In total, 2197 simulations were conducted, exploring combinations of defined parameter value ranges. The best-performing parameter configuration was identified based on Wasserstein distance, marking a substantial improvement over SUMO's default settings and indicating a better alignment between the simulated and observed distributions of travel times. Once the best configuration had been selected from the grid search, an additional robustness test was performed by re-running this configuration with five independent random seeds. The same test was also performed for the default SUMO configuration, in order to compare the calibrated result with the baseline while accounting for simulation stochasticity. The default SUMO configuration produced a Wasserstein distance of W = 11.36 $\pm$ 0.83, reported as mean $\pm$ standard deviation over the five replications. The selected Step 1 configuration reduced the distance to W = 5.59 $\pm$ 0.58, corresponding to an improvement of approximately 50.8% with respect to the default configuration. This confirms that the improvement achieved by the Step 1 calibration is substantially larger than the variability associated with the random simulation seed. The optimal values, differentiated by vehicle class, are as follows:

- Light vehicles: tau = 0.6, actionStepLength = 0.5.
- Motorcycles: tau = 0.6, actionStepLength = 0.5.
- Heavy vehicles: tau = 0.8, actionStepLength = 0.8.
- (speedFactor and minGap were fixed at 1.6 and 3, respectively, based on pre-calibration results).

The optimal values identified show a differentiation consistent with the characteristics of the three vehicle classes. For light vehicles (cars, taxis, medium-sized vehicles), a reduced accepted reaction time (τ = 0.6 s) combined with a rapid decision interval (actionStepLength = 0.5 s) describes reactive and fluid driving behaviour, typical of urban traffic where interactions are frequent and require rapid adjustments. Motorcycles have the same parametric configuration (τ = 0.6 s, ASL = 0.5 s), highlighting an equally dynamic driving style characterised by short response times. This reflects agile mobility and a level of interaction with surrounding traffic similar to that of light vehicles in the context analysed. Heavy vehicles maintain a more anticipatory behaviour, with a higher tau value (τ = 0.8 s) and a longer decision interval (ASL = 0.8 s). This configuration is consistent with their greater inertia, requiring more gradual manoeuvres and more advanced planning. The maintenance of speedFactor = 1.6 and minGap = 3.0 m derives from the evidence of the pre-calibration phase, which showed that these values ensure a stable balance between flow capacity and the absence of abnormal behaviour or unrealistic congestion situations. Overall, the set of calibrated parameters adequately represents the operational differences between vehicle categories, improving the dynamic consistency and plausibility of the simulation model.

In Figure 7, it is possible to observe the notable effect that the calibration had on the simulated travel time distribution, which is now closer to the observed one with respect to the previous phase.

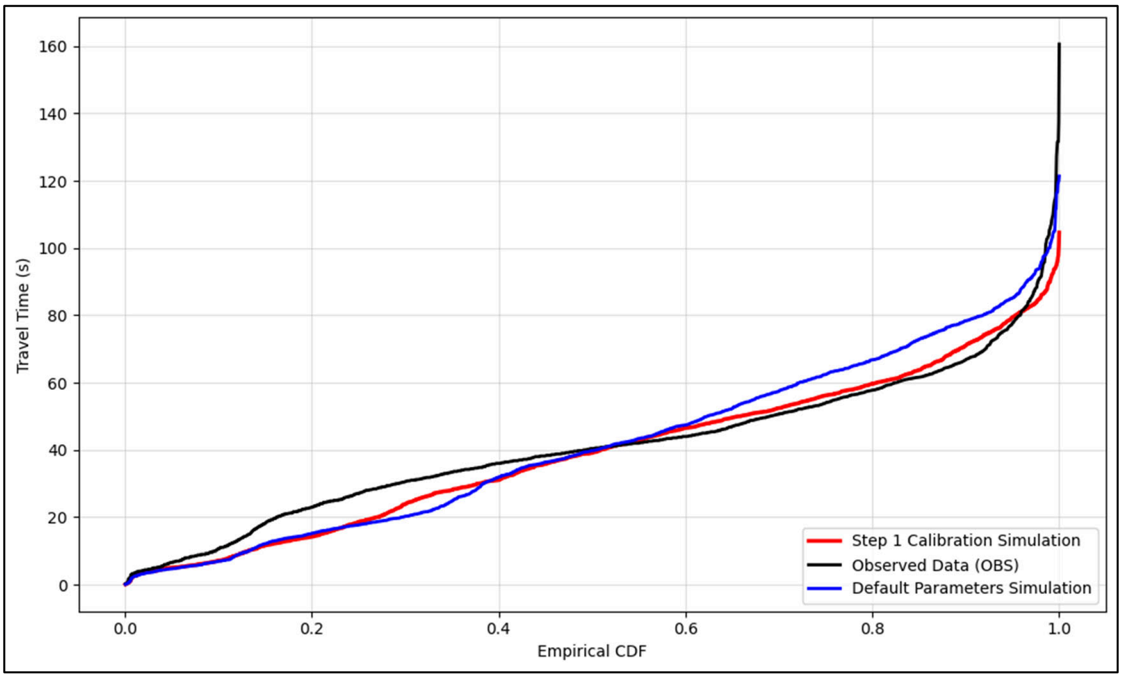

Figure 7. Travel time distributions comparison for all vehicles.

Overall, these results underscore the importance of class-specific calibration, particularly for parameters such as tau, which have a direct impact on interaction timing and vehicle responsiveness. The gains achieved in this phase provide a base for the subsequent steps of the calibration process.

4.2. Step 2—Calibration of Variability-Related Parameters

The second phase calibrated the parameters of variability in vehicle speed and longitudinal behaviour, respectively, speedDev (dispersion of the desired speed around speedFactor) and sigma (driver imperfection, understood as stochastic noise in acceleration and deceleration decisions). The other parameters already optimised in the previous phase (tau, actionStepLength, minGap, speedFactor) were kept fixed to isolate the effect of the behavioral variability component alone. To ensure a robust estimate with respect to the intrinsic randomness of the simulation, linked to the order of vehicle generation, random sampling of speeds, and other micro-fluctuations, each pair of parameters (sigma, speedDev) was evaluated using five independent replicates performed with different seeds of the SUMO random generator. For each replication, the Wasserstein distance between the distributions of simulated and observed travel times was calculated, and the overall performance of the pair of parameters was summarised using the mean and standard deviation of the metric over the five replications. This approach allows for the selection of configurations that are both accurate (low average distance) and stable (low variability between replications), reducing the influence of stochastic effects. In Table 2 a summary of the calibration step is reported.

Table 2. Summary of Calibration Step 2.

Parameter	**Description**	**Default SUMO**	**Tested Range**	**Optimal Configuration (W = 5.27 ± 0.32)**
sigma	The driver imperfection (0 denotes perfect driving)	0.5	0.3–0.7 (step 0.1)	0.3
speedDev	The deviation of the speedFactor	0.1	0–0.20 (step 0.05)	0.05

The optimal value identified corresponds to sigma = 0.3 and speedDev = 0.05. This configuration suggests that a medium-low noise component in car-following dynamics (remembering that sigma = 0 represents perfectly deterministic driving) allows for better reproduction of the natural variability of driver behaviour without compromising the numerical stability of the model. Similarly, a limited dispersion of desired speeds (speedDev = 0.05) allows for a realistic representation of traffic heterogeneity, avoiding excessive differences between vehicles and maintaining consistent flows. The mean Wasserstein distance of the best configuration tested decreased from W = 5.59 ± 0.58 after Step 1 to W = 5.28 ± 0.33 after Step 2. Although the improvement is smaller than the one obtained in the first calibration step, the reduction in both the mean value and the standard deviation indicates that the variability-related parameters improve the stability of the simulated travel time distribution across stochastic replications. Overall, calibration with multiple replications with different seeds reduced sensitivity to random effects and produced a parametric configuration capable of maintaining consistent position and amplitude of the simulated travel time distribution compared to the observed one.

4.3. Step 3—Calibration of Vehicle Dynamic Parameters

In the third calibration step, the focus was placed on vehicle dynamics, specifically the maximum acceleration (accel) and deceleration (decel) values for each vehicle class. These parameters govern how rapidly a vehicle can adjust its speed, influencing its interaction with other vehicles, queue formation and dissipation, and stop-and-go moments around signalised intersections. Keeping the car-following parameters obtained in Step 1 and Step 2 fixed, a grid search was conducted over plausible ranges of "accel" and "decel" values for light vehicles, heavy vehicles, and motorcycles. In total, 5625 simulations were executed, and for each configuration, the simulated travel time distribution was compared to the empirical one. After the best-performing Step 3 configuration was identified, it was re-evaluated using five independent replications with different random seeds. The final calibrated configuration yielded a mean Wasserstein distance of W = 5.02 ± 0.29, further improving the result obtained after Step 2. Overall, the calibration procedure reduced the Wasserstein distance by approximately 55.8% with respect to the default SUMO configuration (W = 11.36 ± 0.83). The limited standard deviation across replications confirms that the improvement is not driven by a single favourable simulation seed. In Table 3, an overview of calibration and results is reported.

Table 3. Summary of Calibration Step 3.

Vehicles Class	Parameter	Default SUMO	Tested Range	Optimal Configuration (W = 5.02 ± 0.29)
Light vehicles	accel	2.6 m/s^2	2.2–3.0 (step 0.2)	2.2 m/s^2
	decel	4.5 m/s^2	4.1–4.9 (step 0.2)	4.3 m/s^2
Motorcycles	accel	6 m/s^2	5.6–6.4 (step 0.2)	6 m/s^2
	decel	10 m/s^2	9.6–10.4 (step 0.2)	10.4 m/s^2
Heavy vehicles	accel	1.3 m/s^2	1.1–1.5 (step 0.2)	1.5 m/s^2
	decel	4 m/s^2	3.8–4.2 (step 0.2)	4.2 m/s^2

The calibration of dynamic parameters (acceleration and deceleration) yields small but significant deviations from SUMO's default values, thereby improving consistency between simulated and observed vehicle behaviour. For light vehicles, the optimal acceleration (2.2 m/s^2) is in the lower range of the tested interval, indicating less aggressive acceleration phases, compatible with an urban context characterised by limited space and frequent speed variations. Deceleration (4.3 m/s^2), slightly below the average value of the tested range, suggests more progressive and distributed braking, consistent with the presence of numerous short-distance interactions and the need to maintain smooth driving in heavy traffic conditions. Motorcycles have acceleration and deceleration values substantially in line with the typical values: accel = 6.0 m/s^2 and decel = 10.4 m/s^2. This configuration reflects a particularly responsive dynamic, typical of vehicles characterised by high agility and the ability to adapt quickly to traffic conditions. The slight preference for higher deceleration helps to better capture the instantaneous corrections typical of motorcycle driving, especially when lateral manoeuvres or sudden changes in surrounding traffic occur. For heavy vehicles, the optimal acceleration (1.5 m/s^2) is consistent with their greater inertia, requiring longer times to reach cruising speeds. The calibrated deceleration (4.2 m/s^2) is at the high end of the tested range, reflecting robust braking capacity and generally more anticipatory driving, as expected for professional drivers accustomed to handling high masses with precision. Overall, the changes are minor but functional in reproducing more stable and realistic vehicle dynamics, improving the model's response to the conditions observed and strengthening the credibility of the simulations in the urban environment analysed. In Figure 8, the comparison between observed and simulated travel times, related to the optimal parameter configuration, is reported per vehicle class. An acceptable alignment is observed for the light vehicles and motorcycle groups, confirming the effectiveness of the calibration process for these vehicle types. However, some localised deviations appear, particularly in the 25–35 s range, which may reflect limitations in capturing mixed-traffic dynamics. In contrast, the heavy vehicles and buses group shows more significant discrepancies, with simulated travel times consistently underestimating the observed ones. This mismatch is likely due to the limited number of vehicles in this class, making the calibration process less robust and less representative for heavy-duty traffic.

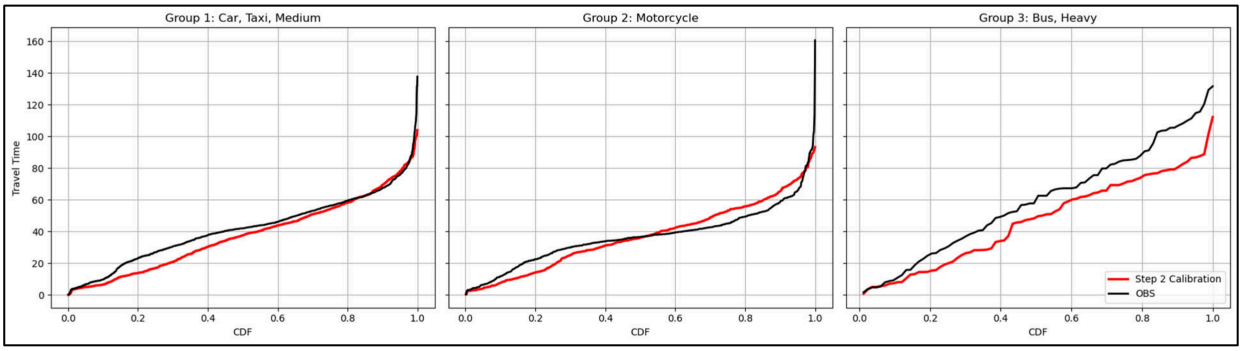

Figure 8. Observed vs. Simulated travel times distribution per vehicle class.

4.4. Lane-Level Microscopic Validation

Following the calibration process, additional microscopic checks were performed to assess the realism of the simulated traffic beyond travel time distributions. Although travel time alignment for individual vehicles represents a key performance indicator, it does not guarantee that local traffic dynamics and interactions are accurately reproduced. For this reason, a lane-level analysis was conducted on the main arterial, focusing on lane-specific flows and headway distributions.

4.4.1. Lane Flow Analysis and Scenario Refinement

The analysis was conducted on a central segment of a selected edge located along the main arterial. On the simulation side, lane-specific vehicle counts were obtained by installing lane-level detectors in SUMO, as shown in Figure 9. On the observation side, the same counts were extracted from the pNEUMA trajectories by filtering vehicles included in the simulation crossing the same section. Table 4 reports the number of vehicle passages per lane. Lane numbering follows the SUMO convention, where lanes are indexed from right to left with respect to the direction of travel. Accordingly, lane 0 denotes the rightmost lane, lane 1 the adjacent lane to its left, and higher lane numbers indicate progressively more leftward lanes. A pronounced mismatch between observed and simulated traffic is evident, particularly for lanes 0 and 1. In the baseline simulation, lane 0 is heavily utilised, whereas in the observed data it is almost entirely avoided, with most vehicles preferentially using lane 1.

Figure 9. The section investigated by simulated data recorded on detectors (yellow shapes) on edge 209871571#0.

Table 4. Vehicle passages per lane comparison.

Lane	Observation		Simulation	
0	20	3%	139	19%
1	123	17%	52	7%
2	166	23%	143	20%
3	233	33%	188	26%
4	171	24%	191	27%

This discrepancy originates from a local traffic dynamic specific to the study area. Although lane 0 is formally available and designated for right-turn movements, drivers tend to avoid it due to frequent temporary stops caused by taxis, delivery vehicles, and short-term parking. This behaviour was confirmed through visual inspection of the site using Google Maps (version 22/05/2024) and Street View. Replicating this dynamic directly in microscopic models is not straightforward for informal or intermittent lane obstructions unless they are explicitly modelled. As a result, lane 0 remains fully available in the baseline simulation and is therefore used unrealistically intensively. To better align simulated behaviour with observed traffic patterns, targeted adjustments were introduced at two consecutive signalised intersections along the main arterial. Specifically, right-turn movements were enabled from lane 1 in addition to lane 0, and the straight-through movement from lane 0 was disabled, effectively restricting this lane to right-turn traffic only. Figure 10 illustrates the original (a) and modified (b) intersection configurations.

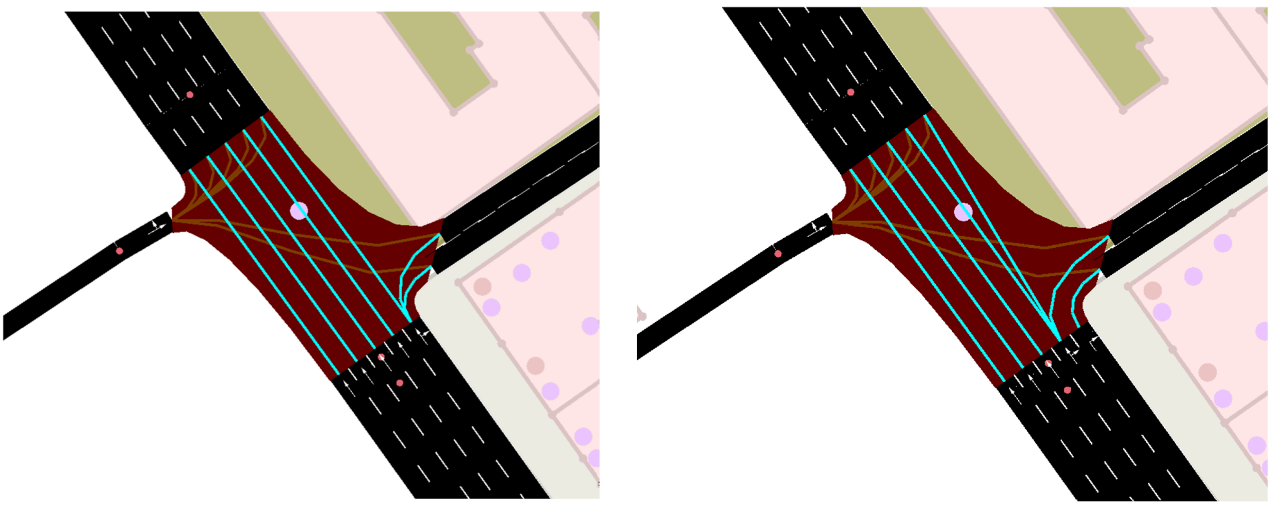

(**a**) (**b**)

Figure 10. Intersection (brown) configuration before (**a**) and after (**b**) the maneuver (blue) refinement.

The simulation performed using the modified network shows a substantial improvement in the lane flow distribution (Table 5). Traffic in the refined scenario makes greater use of lane 1 and reduced use of lane 0, closely reproducing the observed lane usage pattern. Although minor quantitative differences persist, they can be considered within the natural variability expected in a complex urban traffic environment.

The network refinement inevitably affects travel time distributions; however, this impact was limited and primarily associated with very short trips. The Wasserstein distance achieved during the calibration phase remains largely unchanged, indicating that the refined configuration represents a suitable compromise between travel time accuracy and realistic lane-level flow representation.

Table 5. Comparison of observed and simulated lane usage for the analysed section, before and after network refinement.

Lane	Observation		Baseline Simulation		Modified Simulation	
0	20	3%	139	19%	49	7%
1	123	17%	52	7%	134	19%
2	166	23%	143	20%	152	21%
3	233	33%	188	26%	179	25%
4	171	24%	191	27%	199	28%

4.4.2. Headways Analysis

As a further microscopic validation test, headways were analysed in the same section considered in the previous subsection. Headways provide a sensitive measure of vehicle–vehicle interactions and are particularly relevant when the model is subsequently used for road safety analysis. As before, data were collected using lane detectors included in the model and by a local extraction at the specific point from the observed trajectories. The global headway distribution for the entire cross-section is shown in Figure 11, comparing observed and simulated values. The two curves exhibit a similar overall profile, with consistent behaviour across most quantiles and a slight divergence in the upper tail, where low traffic density leads to naturally higher variability.

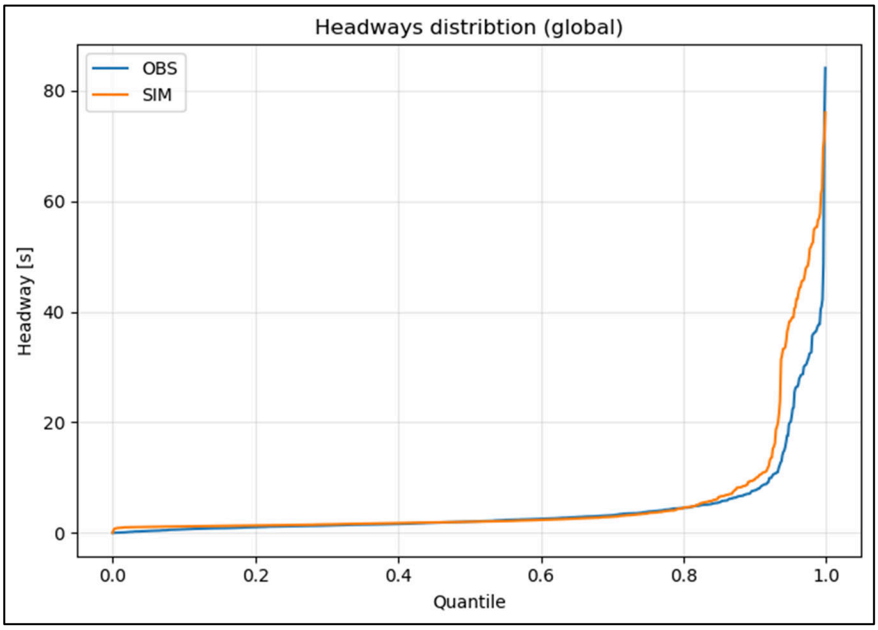

Figure 11. Global headway distributions comparison for the analysed section on edge 209871571#0.

Table 6 reports the average headway per lane. These values provide a more detailed view of lane-specific interactions and allow the assessment of whether the refined scenario reproduces the observed microscopic traffic patterns.

Overall, the values in Table 6 indicate that the refined scenario reproduces lane-specific headways with a satisfactory level of accuracy. Some differences between observed and simulated averages are present, particularly on lane 0, where the simulation still exhibits slightly shorter headways. This behaviour is consistent with the residual tendency of traffic simulation to use lane 0 more than what is observed in the real-world data, despite the improvements introduced by the network refinement. For the remaining lanes, simulated headways closely follow the observed values, although non-negligible differences are still found on lanes 2 and 3, where the simulated average headways are higher than the observed ones. These results indicate that the refined scenario captures the general magnitude of lane-level interactions, but does not fully reproduce all local traffic dynamics. Nevertheless, the lane-level analysis provides useful evidence of the model's ability to represent local traffic patterns and helps identify specific aspects, such as lateral behaviour, that could be further improved in future calibration efforts.

Table 6. Average headway [s] per lane.

Lane	Average Headway [s]	
	Observation	**Simulation**
0	18.580	14.836
1	5.969	6.240
2	3.937	5.326
3	2.824	4.824
4	4.196	4.203

4.4.3. Independent Validation Procedure

To further assess the robustness of the calibrated parameter set, an additional validation experiment was carried out using the observed traffic flow on a different time interval from the same day, in particular from 10:00 to 10:30. The parameters calibrated on the original scenario (08:30–09:00) were applied to this new scenario without any further recalibration. The objective was to verify whether the calibrated configuration could still give an improvement in reproducing the observed travel time distributions with respect to default values. Figure 12 compares the empirical travel time distributions obtained from the observed data, the default simulation, and the simulation using the calibrated parameters in the independent validation scenario. The calibrated configuration provides a clear improvement over the default parameters, as its distribution more closely matches the observed curve over a substantial part of the range. This effect is particularly visible for trips longer than approximately 30–40 s, where travel times are more likely to reflect the combined influence of car-following behaviour, signal delays, queueing, and local interactions. Conversely, very short trips are less informative for assessing behavioural calibration, since their duration is more strongly affected by boundary conditions and local route reconstruction. Overall, the results indicate that the calibrated parameter set retains a positive effect when applied to a different time interval within the same study area, although some discrepancies remain, especially in the upper tail of the distribution.

To better analyse the validation results and reduce the risk that aggregate distributional agreement masks class-specific effects, stratified comparisons by vehicle type were also performed. The results are reported in Table 7. For each vehicle class, the Wasserstein distance was computed over five independent simulation replications, and the table reports the average value obtained for the default and calibrated configurations. The calibrated configuration reduces the Wasserstein distance for all vehicle classes considered in the validation scenario. The largest relative improvements are observed for taxis, medium vehicles, and cars, while motorcycles also show a substantial reduction. Improvements are also obtained for heavy vehicles and buses; however, these two classes represent only a small share of the validation sample, and their results should therefore be interpreted with caution. Overall, the vehicle-type stratification confirms that the positive effect of the calibrated parameters is not limited to the aggregate distribution, but is also reflected across the main traffic components represented in the scenario.

https://doi.org/10.3390/su18147210

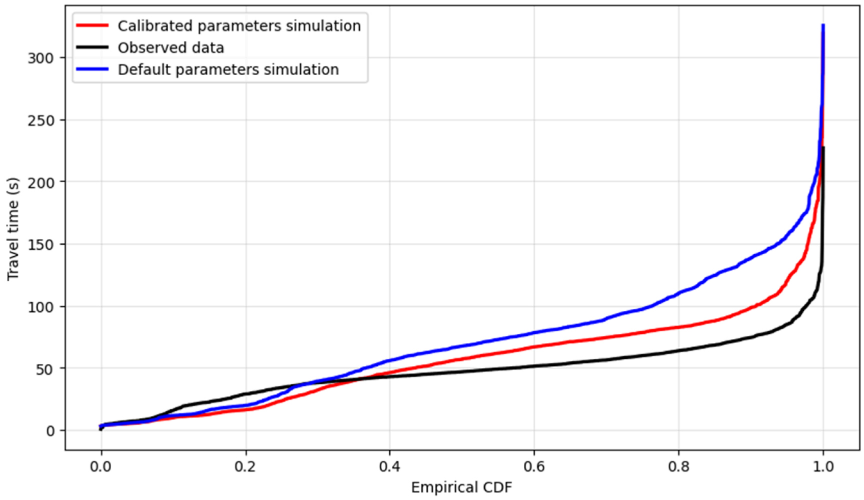

Figure 12. Comparison of travel time distributions between observed data, default parameters and calibrated parameters scenarios.

Table 7. Vehicle-type stratified Wasserstein distance in the independent temporal validation scenario.

Vehicle Type	N Sample	Avg_W_default	Avg_W_calibrated	Improvement Percent
Car	751	23.66	13.18	44%
Medium vehicle	101	21.85	12.02	45%
Taxi	538	24.67	11.33	54%
Motorcycle	860	30.01	16.94	43%
Heavy vehicle	16	13.06	9.78	25%
Bus	40	34.43	20.33	41%

Overall, the independent validation suggests that the calibrated parameters move the model response in the correct direction, also in a different time window.

4.4.4. Effect of Calibration on Emission Estimates

The calibration process aims to improve the realism of simulated traffic dynamics by adjusting the behavioural parameters that govern vehicle interactions, speed adaptation, and acceleration patterns. As a consequence, its effects are not limited to travel time distributions, but can also influence several other simulation outputs derived from vehicle trajectories. Among these, emission estimates are particularly relevant, since microscopic emission models are strongly affected by speed profiles, acceleration and deceleration events, stop-and-go conditions, and the overall temporal evolution of vehicle movements. For this reason, an additional comparison was performed between the outputs obtained from the default parameters scenario and the calibrated configuration. The objective of this analysis is not to validate absolute emission estimates, since no direct field measurements of emissions were available, but to assess the sensitivity of emission-related simulation outputs to the calibration of microscopic behavioural parameters.

Emission outputs were computed using the HBEFA4-based emission model implemented in SUMO. The vehicle categories were mapped to SUMO vehicle classes through the "vClass" attribute without additional fuel-type, Euro-standard, or fleet-composition calibration. Therefore, the emission results should be interpreted as HBEFA4-based simulation outputs used to assess the sensitivity of emission estimates to behavioural calibration, rather than as directly validated absolute emission values. The analysis focuses on tailpipe emissions, including CO2, NOx, and fuel consumption. Table 8 reports the comparison between the default and calibrated configurations. Since both scenarios are based on the same traffic demand and produce the same number of completed vehicles, with an almost identical total travelled distance, the comparison highlights the effect of behavioural calibration on both traffic performance and emission estimates.

Table 8. Total emissions comparison between default parameters and calibrated parameters simulations.

Simulation	Vehicles	Total Distance [km]	Total Travel Time [s]	CO_2 [g]	NOx [g]	Fuel [g]	CO_2 g/km	NOx g/km
DEFAULT	2104	748.12043	130,641	272,438	152.13	88,170	364.16	0.203
CALIBRATED	2104	748.17038	108,526	313,046	193.37	101,293	418.42	0.258
		0%	−17%	15%	27%	15%	15%	27%

The aggregate results reported in Table 8 show that the calibrated configuration produces a clear improvement in traffic performance, with total travel time decreasing by approximately 17% compared with the default configuration. However, the emission-related indicators follow an opposite trend. Total CO_2 emissions and fuel consumption increase by approximately 15%, while NOx emissions increase by about 27%. The same pattern is observed for the distance-normalised indicators, confirming that the increase is not due to longer travelled distances, but rather to changes in the simulated vehicle dynamics. To better understand this behaviour, Figure 13 reports the second-by-second evolution of CO_2 and NOx emissions for the default and calibrated configurations. The temporal profiles show that the calibrated scenario generally produces higher emission rates during most of the active simulation period, especially in the central part of the observation window. This result suggests that the calibrated parameters generate vehicle trajectories that are more consistent with dense urban driving conditions, where frequent speed adjustments, accelerations, decelerations, and stop-and-go interactions are expected. In this scenario, such a more reactive driving behaviour contributes to reducing total travel time, as vehicles are able to complete their trips more quickly. At the same time, however, the same dynamics lead to higher instantaneous emission peaks and, consequently, to higher total emission values. This is particularly evident for NOx, which shows a stronger increase in the calibrated configuration and is highly sensitive to transient driving conditions.

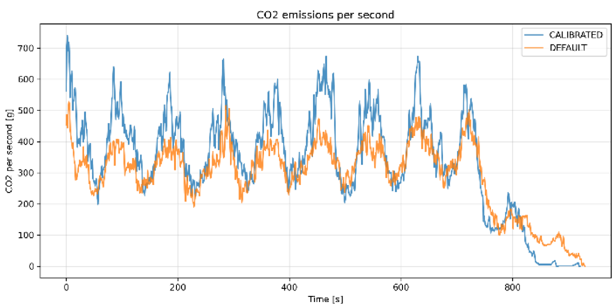

(**a**)

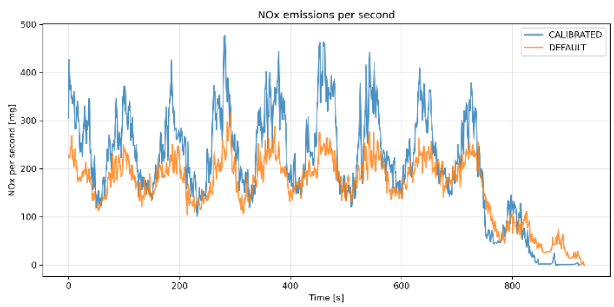

(**b**)

Figure 13. Estimated CO_2 (**a**) and NOx (**b**) emissions per second comparison between default and calibrated configurations.

This result highlights the importance of calibration in refining simulated user behaviour according to the specific characteristics of the scenario and urban context under analysis. The differences observed between the default and calibrated configurations show that environmental results can be strongly influenced by the behavioural parameters adopted in the model. Therefore, when microscopic simulation is used for emission-related analyses, especially in dense urban contexts characterised by frequent accelerations, decelerations, and stop-and-go conditions, calibration becomes important because it can substantially affect the simulated speed and acceleration profiles from which emission estimates are derived.

5. Conclusions

This study proposed a methodology for calibrating microscopic traffic simulation models based on high-resolution vehicle trajectory data. The approach enables a progressive refinement of the model, starting from the definition of the road network and traffic demand directly from observed trajectories and proceeding through a structured, multi-step calibration of singular parameters specifically estimated by vehicle class. A key element of the methodology is the use of the Wasserstein distance to compare simulated and observed travel time distributions from vehicle-level trajectory data, as an alternative to commonly adopted aggregate performance indicators. This choice allows the calibration process to capture fine-grained behavioural variability and to consistently improve the alignment between simulated dynamics and those observed in real data, highlighting the importance of distribution-based calibration approaches over mean-value matching. The results also indicate that using travel time distributions as an indicator to compare simulated and observed situations, while useful to adjust traffic simulation parameters, is not sufficient to ensure realism at the local level of a microscopic traffic simulation model. In particular, traffic distribution among lanes may remain undetected when validation relies exclusively on travel time metrics. For this reason, the proposed workflow integrates additional validation steps, such as lane-level flow analysis and headway evaluation at specific points. These complementary checks proved their value for identifying discrepancies that would not have emerged from travel-time analysis alone and for guiding targeted refinements of both the network configuration and the calibrated parameters. Finally, the comparison between default and calibrated configurations also showed that behavioural calibration can substantially affect emission estimates. This confirms that calibrated microscopic models are not only useful for reproducing traffic performance indicators, but also for supporting sustainability-oriented analyses, where environmental outputs depend directly on the simulated vehicle dynamics. In this perspective, refining road-user behaviour according to the specific urban context becomes essential to obtain more realistic estimates of both traffic and emission-related indicators.

Despite these contributions, some limitations should be acknowledged. First, the calibration was performed on a specific urban area and observation interval, while the independent validation was limited to a different time period within the same study area. Therefore, the results support temporal robustness within the analysed network, but cannot confirm full spatial transferability to other zones or cities. Second, lane-changing parameters were kept fixed during calibration, which may partly explain the remaining discrepancies in lane-specific flows and headways. Third, the emission analysis was not validated against direct field emission measurements; consequently, the reported emission values should be interpreted as simulation-based outputs useful for assessing the sensitivity of environmental indicators to behavioural calibration, rather than as absolute validated emission levels. Future work should extend the proposed workflow to multiple areas, longer observation periods, explicit calibration of lateral behaviour, and direct validation of emission-related outputs where suitable field measurements are available.

Overall, the developed methodology provides a structured and reproducible workflow based on open-source tools, which can support future applications in other urban contexts where high-resolution trajectory data are available. Nevertheless, context-specific calibration and validation remain necessary before transferring calibrated parameter values to different networks or traffic conditions. The approach is particularly suited for dense, signalised urban networks, where detailed observation of vehicle interactions and temporal dynamics is critical for realistic model calibration. Future work will focus on assessing the transferability of the calibrated parameters across different periods of the day and on other parts of the network for extending the validation framework. Also, additional microscopic indicators can be used to support advanced applications such as road safety solutions.

Author Contributions: Conceptualization, L.S., F.D., M.F. and G.C.; methodology, L.S., F.D., M.F. and G.C.; software, L.S. and M.F.; validation, L.S., F.D., M.F. and G.C.; formal analysis, L.S., F.D., M.F. and G.C.; investigation, L.S., F.D., M.F. and G.C.; resources, L.S., F.D., M.F. and G.C.; data curation, L.S. and M.F.; writing—original draft preparation, L.S., F.D., M.F. and G.C.; writing—review and editing, L.S., F.D., M.F. and G.C.; visualization, L.S., F.D., M.F. and G.C.; supervision, F.D.; project administration, F.D.; funding acquisition, F.D. All authors have read and agreed to the published version of the manuscript.

Funding: This research received no external funding.

Institutional Review Board Statement: Not applicable.

Informed Consent Statement: Not applicable.

Data Availability Statement: The original data presented in the study are openly available in "Pneuma Open Traffic" at "https://open-traffic.epfl.ch/" (accessed on 4 July 2026).

Acknowledgments: The authors gratefully acknowledge the pNEUMA team for granting access to the pNEUMA Dataset. The authors thank the SUMO development team for making their open-source traffic simulation tool available.

Conflicts of Interest: The authors declare no conflicts of interest.

References

1. Kan, Z.; Tang, L.; Kwan, M.-P.; Ren, C.; Liu, D.; Li, Q. Traffic Congestion Analysis at the Turn Level Using Taxis' GPS Trajectory Data. *Comput. Environ. Urban Syst.* **2019**, *74*, 229–243. [CrossRef]
2. Tang, L.; Kan, Z.; Zhang, X.; Yang, X.; Huang, F.; Li, Q. Travel Time Estimation at Intersections Based on Low-Frequency Spatial-Temporal GPS Trajectory Big Data. *Cartogr. Geogr. Inf. Sci.* **2016**, *43*, 417–426. [CrossRef]
3. Tian, X.; Zhang, W.; Yang, Z.-S.; Zhou, X.; Bing, Q. Urban Link Travel Time Estimation Based on Low Frequency Probe Vehicle Data. *Discret. Dyn. Nat. Soc.* **2016**, *2016*, 7348705. [CrossRef]
4. Vincke, B.; Michel, P.; Ouardi, A.E.; Larnaudie, B.; Delgehier, F.; Sadoun, R.; Bouaziz, S.; Espié, S.; Rodriguez, S.; Boubezoul, A. Real Track Experiment Dataset for Motorcycle Rider Behavior and Trajectory Reconstruction. *Data Brief.* **2024**, *57*, 111026. [CrossRef] [PubMed]
5. Kumari, S.; Ghai, S.; Kushwaha, B. Vehicle and Object Tracking Based on GPS and GSM. *Int. J. Nov. Res. Comput. Sci. Softw. Eng.* **2016**, *3*, 255–259.
6. Tang, L.; Yang, X.; Kan, Z.; Li, Q. Lane-Level Road Information Mining from Vehicle GPS Trajectories Based on Naïve Bayesian Classification. *ISPRS Int. J. Geo-Inf.* **2015**, *4*, 2660–2680. [CrossRef]
7. Cao, X.; Lan, J.; Li, X.R.; Liu, Y. Automotive Radar-Based Vehicle Tracking Using Data-Region Association. *IEEE Trans. Intell. Transp. Syst.* **2022**, *23*, 8997–9010. [CrossRef]
8. Wang, J.; Fu, T.; Xue, J.; Li, C.; Song, H.; Xu, W.; Shangguan, Q. Realtime Wide-Area Vehicle Trajectory Tracking Using Millimeter-Wave Radar Sensors and the Open TJRD TS Dataset. *Int. J. Transp. Sci. Technol.* **2023**, *12*, 273–290. [CrossRef]
9. Gao, Y.; Zhou, C.; Rong, J.; Wang, Y. High-Accurate Vehicle Trajectory Extraction and Denoising from Roadside LIDAR Sensors. *Infrared Phys. Technol.* **2023**, *134*, 104896. [CrossRef]
10. Gong, B.; Zhao, B.; Wang, Y.; Lin, C.; Liu, H. Vehicle Trajectory Extraction with Interacting Multiple Model for Low-Channel Roadside LiDAR. *Expert Syst. Appl.* **2025**, *262*, 125662. [CrossRef]

11. Tang, J.; Wang, W. Vehicle Trajectory Extraction and Integration from Multi-Direction Video on Urban Intersection. *Displays* **2024**, *85*, 102834. [CrossRef]
12. Tang, Z.; Naphade, M.; Liu, M.-Y.; Yang, X.; Birchfield, S.; Wang, S.; Kumar, R.; Anastasiu, D.; Hwang, J.-N. CityFlow: A City-Scale Benchmark for Multi-Target Multi-Camera Vehicle Tracking and Re-Identification. In *Proceedings of the 2019 IEEE/CVF Conference on Computer Vision and Pattern Recognition (CVPR), Long Beach, CA, USA, 15–20 June 2019*; IEEE: New York, NY, USA, 2019; pp. 8789–8798.
13. Babinec, A.; Apeltauer, J. On Accuracy of Position Estimation from Aerial Imagery Captured by Low-Flying UAVs. *Int. J. Transp. Sci. Technol.* **2016**, *5*, 152–166. [CrossRef]
14. Barmpounakis, E.N.; Vlahogianni, E.I.; Golias, J.C. Unmanned Aerial Aircraft Systems for Transportation Engineering: Current Practice and Future Challenges. *Int. J. Transp. Sci. Technol.* **2016**, *5*, 111–122. [CrossRef]
15. Kamga, C.; Sapphire, J.; Cui, Y.; Moghimidarzi, B.; Khryashchev, D.; City University of New York; University Transportation Research Center. *Exploring Applications for Unmanned Aerial Systems (UAS) and Unmanned Ground Systems (UGS) in Enhanced Incident Management, Bridge Inspection, and Other Transportation Related Operations: Final Report*; City University of New York: New York, NY, USA; University Transportation Research Center: New York, NY, USA, 2017.
16. Rosenfeld, A. Are Drivers Ready for Traffic Enforcement Drones? *Accid. Anal. Prev.* **2019**, *122*, 199–206. [CrossRef] [PubMed]
17. Wang, Z.; Yu, Z.; Tian, W.; Xiong, L.; Tang, C.; Wang, Z.; Yu, Z.; Tian, W.; Xiong, L.; Tang, C. *A Method for Building Vehicle Trajectory Data Sets Based on Drone Videos*; SAE International: Warrendale, PA, USA, 2023.
18. Barmpounakis, E.; Geroliminis, N. On the New Era of Urban Traffic Monitoring with Massive Drone Data: The *pNEUMA* Large-Scale Field Experiment. *Transp. Res. Part C Emerg. Technol.* **2020**, *111*, 50–71. [CrossRef]
19. Kaufmann, S.; Kerner, B.S.; Rehborn, H.; Koller, M.; Klenov, S.L. Aerial Observations of Moving Synchronized Flow Patterns in Over-Saturated City Traffic. *Transp. Res. Part C Emerg. Technol.* **2018**, *86*, 393–406. [CrossRef]
20. Ke, R.; Li, Z.; Tang, J.; Pan, Z.; Wang, Y. Real-Time Traffic Flow Parameter Estimation from UAV Video Based on Ensemble Classifier and Optical Flow. *IEEE Trans. Intell. Transp. Syst.* **2019**, *20*, 54–64. [CrossRef]
21. Moers, T.; Vater, L.; Krajewski, R.; Bock, J.; Zlocki, A.; Eckstein, L. The exiD Dataset: A Real-World Trajectory Dataset of Highly Interactive Highway Scenarios in Germany. In Proceedings of the 2022 IEEE Intelligent Vehicles Symposium (IV), Aachen, Germany, 5–9 June 2022; pp. 958–964.
22. Pan, C.; Dai, Z.; Zhang, Y.; Zhang, H.; Fan, M.; Xu, J. An Approach for Accurately Extracting Vehicle Trajectory from Aerial Videos Based on Computer Vision. *Measurement* **2025**, *242*, 116212. [CrossRef]
23. Jiao, Y.; Calvert, S.C.; van Cranenburgh, S.; van Lint, H. Inferring Vehicle Spacing in Urban Traffic from Trajectory Data. *Transp. Res. Part C Emerg. Technol.* **2023**, *155*, 104289. [CrossRef]
24. Yang, Z.; Zheng, Z.; Kim, J.; Rakha, H. Eco-Driving Strategies Using Reinforcement Learning for Mixed Traffic in the Vicinity of Signalized Intersections. *Transp. Res. Part C Emerg. Technol.* **2024**, *165*, 104683. [CrossRef]
25. Wang, J.; Zhang, Z.; Lu, G. Calibration and Analysis of Heterogeneous Car-Following Behaviors Based on a Naturalistic Trajectory Dataset on Highways. In *CICTP 2020: Transportation Evolution Impacting Future Mobility*; American Society of Civil Engineers: Reston, VA, USA, 2020; pp. 4279–4290. [CrossRef]
26. Wu, D.; Lee, J.J.; Li, Y.; Jin, J. Exploring Driving Behavioral Characteristics in Pre-, in-, and Post-Conflict Stages Based on Car-Following Trajectory Data. *Ergonomics* **2024**, *68*, 1025–1042. [CrossRef] [PubMed]
27. Gu, R.; Li, Y.; Cen, X. Exploring the Stimulative Effect on Following Drivers in a Consecutive Lane Change Using Microscopic Vehicle Trajectory Data. *Transp. Saf. Environ.* **2023**, *5*, tdac047. [CrossRef]
28. He, Y.; Wang, P.; Chan, C.-Y. Understanding Lane Change Behavior Under Dynamic Driving Environment Based on Real-World Traffic Dataset. In Proceedings of the 2019 5th International Conference on Transportation Information and Safety (ICTIS), Liverpool, UK, 14–17 July 2019; pp. 1092–1097.
29. Wei, H.; Ma, Z.; Zhu, X.; Lin, Y. Characteristics Analysis and Classification of Lane-Changing Behavior after Following Process Based on China-FOT. In Proceedings of the 2019 IEEE Intelligent Vehicles Symposium (IV), Paris, France, 9–12 June 2019; pp. 523–528.
30. Chen, T.; Shi, X.; Wong, Y.D. Key Feature Selection and Risk Prediction for Lane-Changing Behaviors Based on Vehicles' Trajectory Data. *Accid. Anal. Prev.* **2019**, *129*, 156–169. [CrossRef] [PubMed]
31. Xing, L.; He, J.; Abdel-Aty, M.; Cai, Q.; Li, Y.; Zheng, O. Examining Traffic Conflicts of up Stream Toll Plaza Area Using Vehicles' Trajectory Data. *Accid. Anal. Prev.* **2019**, *125*, 174–187. [CrossRef] [PubMed]
32. Espadaler-Clapés, J.; Barmpounakis, E.; Geroliminis, N. Traffic Congestion and Noise Emissions with Detailed Vehicle Trajectories from UAVs. *Transp. Res. Part Transp. Environ.* **2023**, *121*, 103822. [CrossRef]
33. Khan, M.; Ectors, W.; Bellemans, T.; Janssens, D.; Wets, G. Unmanned Aerial Vehicle-Based Traffic Analysis: A Case Study for Shockwave Identification and Flow Parameters Estimation at Signalized Intersections. *Remote Sens.* **2018**, *10*, 458. [CrossRef]
34. Li, L.; Jiang, R.; He, Z.; Chen, X.; Zhou, X. Trajectory Data-Based Traffic Flow Studies: A Revisit. *Transp. Res. Part C Emerg. Technol.* **2020**, *114*, 225–240. [CrossRef]

35. Chowdhury, M.M.H.; Chakraborty, T. Calibration of SUMO Microscopic Simulation for Heterogeneous Traffic Condition: The Case of the City of Khulna, Bangladesh. *Transp. Eng.* **2024**, *18*, 100281. [CrossRef]
36. Cantisani, G.; Serrone, G.D.; Biagio, G.D. Calibration and Validation of and Results from a Micro-Simulation Model to Explore Drivers' Actual Use of Acceleration Lanes. *Simul. Model. Pract. Theory* **2018**, *89*, 82–99. [CrossRef]
37. Figueiredo, M.; Seco, Á.; Silva, A.B. Calibration of Microsimulation Models—The Effect of Calibration Parameters Errors in the Models' Performance. *Transp. Res. Procedia* **2014**, *3*, 962–971. [CrossRef]
38. Saad, S.; Ossart, F.; Bigeon, J.; Sourdille, E.; Gance, H. Global Sensitivity Analysis Applied to Traffic Rescheduling in Case of Power Shortage. *Int. J. Transp. Dev. Integr.* **2017**, *2*, 271–283. [CrossRef]
39. Punzo, V.; Montanino, M. Speed or Spacing? Cumulative Variables, and Convolution of Model Errors and Time in Traffic Flow Models Validation and Calibration. *Transp. Res. Part B Methodol.* **2016**, *91*, 21–33. [CrossRef]
40. Gallelli, V.; Guido, G.; Vitale, A.; Vaiana, R. Effects of Calibration Process on the Simulation of Rear-End Conflicts at Roundabouts. *J. Traffic Transp. Eng. Engl. Ed.* **2019**, *6*, 175–184. [CrossRef]
41. Ranpura, P.; Gujar, R.; Singh, S. Development of Mixed Traffic Microsimulation Model Calibration for Signalized Intersections. *Transp. Res. Procedia* **2025**, *82*, 2898–2910. [CrossRef]
42. Gao, Y.; Zhou, C.; Rong, J.; Zhang, X.; Wang, Y. Enhancing Parameter Calibration for Micro-Simulation Models: Investigating Improvement Methods. *Simul. Model. Pract. Theory* **2024**, *134*, 102950. [CrossRef]
43. Maheshwary, P.; Bhattacharyya, K.; Maitra, B.; Boltze, M. A Methodology for Calibration of Traffic Micro-Simulator for Urban Heterogeneous Traffic Operations. *J. Traffic Transp. Eng. Engl. Ed.* **2020**, *7*, 507–519. [CrossRef]
44. Alarcón, H.L.; Escalante, L.E.B.; Bizarro, R.G.A.; Huamani, A.S.I.; Anaya, R.G.B.; Gamboa, A.T.; Saez, E.C.G.; Fernández, S.W.R.; Tenorio-Huarancca, D.O. Calibration of a Mesoscopic Simulation Model for the Optimization of Traffic Performance Parameters in a Commercial District. *Int. J. Transp. Dev. Integr.* **2025**, *9*, 700–721. [CrossRef]
45. Zhao, J.; Xia, Y.; Wang, C.; Odawa, J. Do the Sparser Access Points Have Less Impact on Arterial Traffic? A Microscopic Simulation-Based Study. *Simul. Model. Pract. Theory* **2025**, *138*, 103036. [CrossRef]
46. Igene, M.; Luo, Q.; Jimee, K.; Soltanirad, M.; Bataineh, T.; Liu, H. Integrating LiDAR Sensor Data into Microsimulation Model Calibration for Proactive Safety Analysis. *Sensors* **2024**, *24*, 4393. [CrossRef] [PubMed]
47. Varga, B.; Doba, D.; Tettamanti, T. Optimizing Vehicle Dynamics Co-Simulation Performance by Introducing Mesoscopic Traffic Simulation. *Simul. Model. Pract. Theory* **2023**, *125*, 102739. [CrossRef]
48. Guo, Y.; Sayed, T.; Zheng, L.; Essa, M. An Extreme Value Theory Based Approach for Calibration of Microsimulation Models for Safety Analysis. *Simul. Model. Pract. Theory* **2021**, *106*, 102172. [CrossRef]
49. Argota Sánchez-Vaquerizo, J. Getting Real: The Challenge of Building and Validating a Large-Scale Digital Twin of Barcelona's Traffic with Empirical Data. *ISPRS Int. J. Geo-Inf.* **2022**, *11*, 24. [CrossRef]
50. Codeca, L.; Jakob, E.; Vinny, C.; Jerome, H. SAGA: An Activity-Based Multi-Modal Mobility ScenarioGenerator for SUMO. *SUMO Conf. Proc.* **2022**, *1*, 39–58. [CrossRef]
51. Lobo, S.; Neumeier, S.; Fernandez, E.M.G.; Facchi, C. InTAS—The Ingolstadt Traffic Scenario for SUMO. *SUMO Conf. Proc.* **2022**, *1*, 73–92. [CrossRef]
52. Rapelli, M.; Casetti, C.; Gagliardi, G. TuST: From Raw Data to Vehicular Traffic Simulation in Turin. In Proceedings of the 2019 IEEE/ACM 23rd International Symposium on Distributed Simulation and Real Time Applications (DS-RT), Rende (CS), Cosenza, Italy, 7–9 October 2019; pp. 1–8.
53. Schweizer, J.; Poliziani, C.; Rupi, F.; Morgano, D.; Magi, M. Building a Large-Scale Micro-Simulation Transport Scenario Using Big Data. *ISPRS Int. J. Geo-Inf.* **2021**, *10*, 165. [CrossRef]
54. Bieker, L.; Krajzewicz, D.; Morra, A.; Michelacci, C.; Cartolano, F. Traffic Simulation for All: A Real World Traffic Scenario from the City of Bologna. In *Proceedings of the Modeling Mobility with Open Data*; Behrisch, M., Weber, M., Eds.; Springer International Publishing: Cham, Switzerland, 2015; pp. 47–60.
55. McKenney, D.; White, T. Distributed and Adaptive Traffic Signal Control within a Realistic Traffic Simulation. *Eng. Appl. Artif. Intell.* **2013**, *26*, 574–583. [CrossRef]
56. Soares, J.; Lobo, C.; Vale, Z.; de Moura Oliveira, P.B. Realistic Traffic Scenarios Using a Census Methodology: Vila Real Case Study. In Proceedings of the 2014 IEEE PES General Meeting | Conference & Exposition, National Harbor, MA, USA, 27–31 July 2014; pp. 1–5.
57. Wang, S.; Zhang, F.; Qin, T. Research on the Construction of Highway Traffic Digital Twin System Based on 3D GIS Technology. *J. Phys. Conf. Ser.* **2021**, *1802*, 42045. [CrossRef]
58. Li, Y.; Zhang, W. Traffic Flow Digital Twin Generation for Highway Scenario Based on Radar-Camera Paired Fusion. *Sci. Rep.* **2023**, *13*, 642. [CrossRef] [PubMed]
59. Liu, C.; Zhang, C.; Wang, B.; Tang, Z.; Xie, Z. Digital Twin of Highway Entrances and Exits: A Traffic Risk Identification Method. *IEEE J. Radio Freq. Identif. Online* **2022**, *6*, 934–937. [CrossRef]

60. Kumarasamy, V.K.; Saroj, A.J.; Liang, Y.; Wu, D.; Hunter, M.P.; Guin, A.; Sartipi, M. Integration of Decentralized Graph-Based Multi-Agent Reinforcement Learning with Digital Twin for Traffic Signal Optimization. *Symmetry* **2024**, *16*, 448. [CrossRef]
61. Liao, X.; Leng, S.; Sun, Y.; Zhang, K.; Ali Imran, M. A Digital-Twin-Based Traffic Guidance Scheme for Autonomous Driving. *IEEE Internet Things J.* **2024**, *11*, 36829–36840. [CrossRef]
62. Wang, W.; He, F.; Li, Y.; Tang, S.; Li, X.; Xia, J.; Lv, Z. Data Information Processing of Traffic Digital Twins in Smart Cities Using Edge Intelligent Federation Learning. *Inf. Process. Manag.* **2023**, *60*, 103171. [CrossRef]
63. Catalano, M.; Lavenant, H.; Lijoi, A.; Prünster, I. A Wasserstein Index of Dependence for Random Measures. *J. Am. Stat. Assoc.* **2024**, *119*, 2396–2406. [CrossRef]